Hemodynamic Effects of Virtual Stenting in the Fontan Circulation at Rest and During Exercise

by

Isaias Sergio Martinez

under the supervision of Dr. Alison Marsden,
Department of Bioengineering, Stanford University

April 2026

Hemodynamic Effects of Virtual Stenting in the Fontan Circulation at Rest and During Exercise

by

Isaias Sergio Martinez

April 2026

Approved:

Alison Marsden 4/24/26

Dr. Alison Marsden Date

Faculty Research Advisor from the Department of Bioengineering

Approved:

4/27/26

Dr. Shiraz Maskatia Date

Faculty Reader from the Department of Pediatrics – Cardiology

Approved:

Karl Deisseroth 06/09/26

Karl Deisseroth, Ph.D., M.D.

Chair for Undergraduate Education in the Department of Bioengineering Date

An Honors Thesis Submitted to the Department of Bioengineering in partial fulfillment of the Honors Program

Acknowledgements

I would like to sincerely thank Dr. Alison Marsden for the opportunity to conduct research in her lab and for allowing me to work on such a meaningful and challenging project. I am deeply grateful for the intellectual environment she has created, one that encourages curiosity, rigor, and thoughtful scientific inquiry. Being part of her lab has been an invaluable experience in my growth as both a student and a researcher.

I would also like to thank Dr. Shiraz Maskatia for generously giving his time and expertise to read this thesis. I am very appreciative of his willingness to serve as a reader and for the thoughtful attention he has given to this work. His clinical perspective and support are greatly valued.

I am especially thankful to Bryan Junhyuk Hwang for his collaboration, guidance, and constant support throughout this project. Bryan has been instrumental at every stage of this work, from helping shape the project to walking through technical details and offering thoughtful advice along the way. I am particularly grateful for his patience in answering my many questions and for the generosity with which he shared his time and knowledge. His mentorship and encouragement made this project possible and far more rewarding.

I am also deeply grateful to Zinan Hu for her mentorship, feedback, and help throughout this project. Her insight and guidance were invaluable, and I greatly appreciated the care she took in providing thoughtful comments and helping me improve both the work itself and how I communicated it. I am very thankful for her support and for the time she invested in helping me learn.

Contents

List of Tables

List of Figures

Abstract

The Fontan circulation is vulnerable to hemodynamic inefficiency because systemic venous return reaches the pulmonary arteries without a subpulmonary ventricle. As a result, even modest pathway narrowing may increase pressure burden and worsen exercise intolerance. Although transcatheter stenting is used to enlarge obstructed Fontan pathways, its hemodynamic benefit is not fully characterized and may vary across patients. The objective of this study was to use patient-specific computational fluid dynamics to evaluate the hemodynamic impact of virtual stenting in Fontan patients under resting and exercise conditions.

Three-dimensional Fontan models were reconstructed from 4D flow MRI data using an image-based SimVascular workflow. Virtual post-stent geometries were generated using svMorph by enlarging the selected pathway segment to eliminate focal narrowing. For each patient, pre-stent and post-stent models were simulated under resting and exercise conditions. Primary outcomes were pressure drop, power loss, and resistance.

The simulations showed that the hemodynamic effect of virtual stenting was strongly patient-specific. In Patients 21 and 23, virtual stenting reduced pressure drop, power loss, and resistance at both rest and during exercise, with the largest reductions in pressure drop and resistance observed during exercise. In Patient 18, the response was more mixed: pressure drop and resistance improved, but power loss increased at both physiologic states, indicating that apparent geometric narrowing alone does not guarantee uniform hemodynamic benefit after pathway enlargement.

These findings suggest that the benefit of Fontan pathway stenting depends on the interaction between local narrowing, overall pathway geometry, and physiologic demand. More broadly, this work supports patient-specific computational modeling as a tool for evaluating whether a given Fontan patient is likely to derive meaningful hemodynamic benefit from stenting.

1 Introduction

1.1 Congenital heart disease and single-ventricle physiology

Congenital heart disease (CHD) is one of the most common congenital abnormalities worldwide, affecting approximately 8–10 per 1,000 live births.[1] Among the many forms of CHD, single-ventricle malformations represent a particularly severe subgroup in which only one ventricle is capable of sustaining the circulation.[2] Because normal biventricular physiology cannot be restored in these patients, treatment relies on staged palliative reconstruction rather than definitive anatomic repair.[2]

The Fontan operation is the final stage of this palliation. Since its introduction in 1971 and subsequent refinement into the modern total cavopulmonary connection, the Fontan strategy has allowed many children with previously fatal forms of CHD to survive into adolescence and adulthood.[3] This success has produced a growing population living with Fontan physiology, shifting clinical focus from early postoperative survival toward the long-term hemodynamic and systemic consequences of this circulation.[3]

1.2 The Fontan Circulation

Despite this major advance, the Fontan circulation remains intrinsically non-physiologic. In its modern form, systemic venous return is directed from the superior and inferior vena cavae to the pulmonary arteries without the aid of a subpulmonary ventricle, creating a total cavopulmonary connection in which pulmonary blood flow depends on passive transpulmonary flow.[3–5] Because forward flow is no longer actively driven by a pumping chamber, adequate pulmonary perfusion must be sustained by elevated systemic venous pressure while ventricular preload remains chronically limited.[4,6,7]

This combination of venous congestion and relatively low cardiac output underlies the “Fontan paradox” and drives many of the long-term complications seen in this population, including exercise intolerance, arrhythmias, protein-losing enteropathy, plastic bronchitis, and Fontan- associated liver disease.[3,4,6,7] Unlike a normal biventricular circulation, the Fontan circulation operates close to its phys-

iologic limits and has little reserve to compensate for added resistance or flow disturbance.[4,7]

Energy loss, resistance, and pressure drop are therefore central hemodynamic concerns in Fontan physiology. de Leval and colleagues demonstrated early on that cavities, sharp turns, and stenotic regions increase energy dissipation, motivating the streamlined designs used in modern Fontan surgery.[5] Power loss quantifies the mechanical energy dissipated across the total cavopulmonary connection, while pressure drop reflects the driving pressure required to sustain flow through the pathway at a given flow rate.[8,9] Both are clinically important: greater resistance or power loss requires higher upstream venous pressure to maintain pulmonary blood flow, worsening the characteristic tradeoff of venous congestion and reduced effective preload.[4,8,9] These relationships are summarized conceptually in the pressure–flow framework shown in Figure 1.

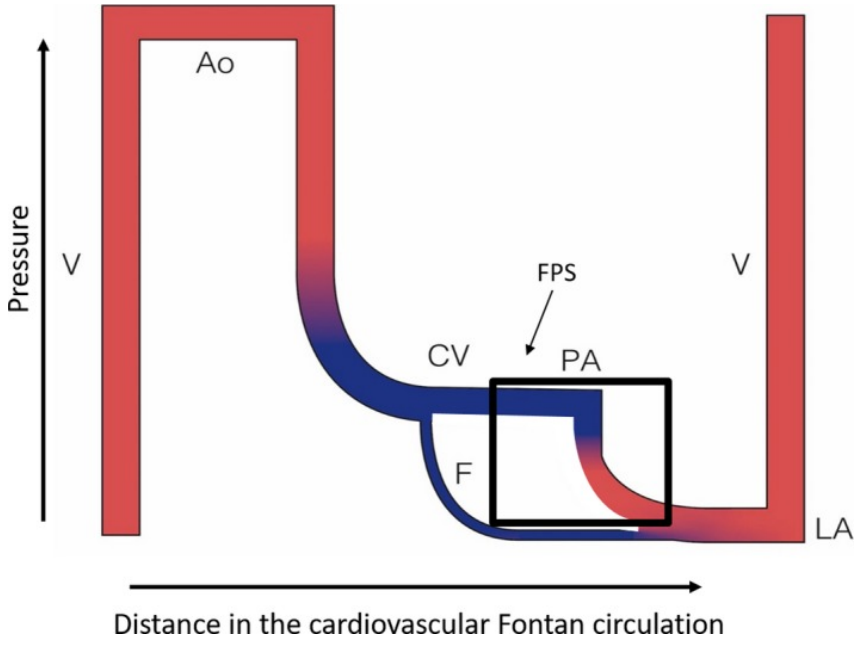

Figure 1: Flow/pressure diagram of the Fontan circulation, plotting pressure as a function of distance through the cardiovascular circuit. The black rectangle highlights the Fontan portal system (FPS), where systemic venous return passes directly from the caval veins to the pulmonary arteries without a subpulmonary ventricle. Ao, aorta; F, Fontan connection; LA, left atrium; V, single ventricle. Adapted from Gewillig et al.[10] under CC BY-NC 4.0.

These limitations become especially consequential during exercise. In a normal circulation, increasing metabolic demand is met by augmenting venous return, pulmonary blood flow, and ventricular preload. In Fontan patients, that response is constrained, limiting the ability to increase stroke volume and cardiac output.[11,12] Power loss within the total cavopulmonary connection increases nonlinearly with cardiac output, and patient-specific simulations under stress conditions confirm that adverse geometry becomes substantially more consequential at higher flows.[13,14] Inefficiencies that appear modest at rest can therefore become more pronounced under higher-flow conditions, which is why exercise intolerance is common in this population and why hemodynamic assessment under both rest and exercise conditions is clinically relevant.[11,12,14,15]

1.3 Conduit Narrowing and Stenting in Fontan Patients

Although the modern total cavopulmonary connection was developed to improve flow efficiency, late obstruction within the Fontan pathway remains a recognized problem. Narrowing may arise from fixed conduit size in a growing child, geometric distortion, calcification or shrinkage of older conduit materials, or focal stenosis within the pathway itself.[16,17] Thus, a pathway that was initially adequate may become relatively undersized over time and produce progressively less favorable hemodynamics,[16,18] particularly within the extracardiac total cavopulmonary connection illustrated in Figure 2.

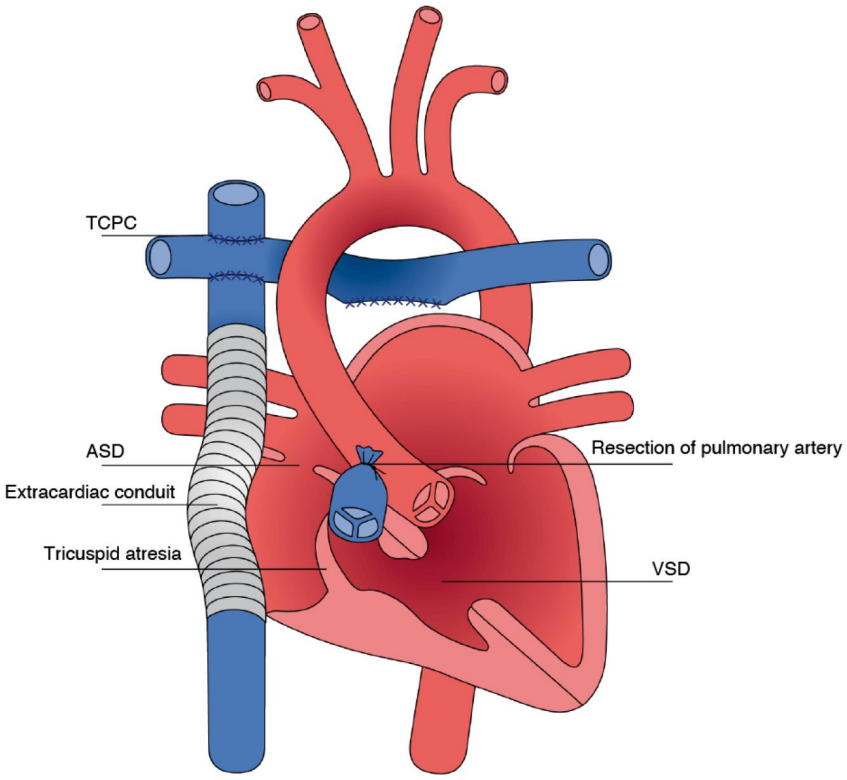

Figure 2: Schematic of the total cavopulmonary connection (TCPC) showing the SVC, IVC, extracardiac conduit, and branch pulmonary arteries.

Transcatheter stenting has therefore become an important strategy for relieving Fontan pathway obstruction. The clinical rationale is straightforward: enlarging a narrowed segment reduces local resistance, decreases pressure loss across the pathway, and improves forward venous flow to the pulmonary arteries.[17,19] Prior clinical series support this approach. In a pediatric cohort with obstructed extracardiac conduits, stenting was successful in all children, significantly increased conduit diameter, and was associated with acute clinical benefit in nearly all cases.[19] More recent adult data showed that percutaneous Fontan stenting significantly reduced Fontan gradient while increasing minimal pathway diameter, with symptomatic improvement in a subset of patients.[20]

At the same time, the magnitude and durability of hemodynamic benefit remain incompletely defined. Much of the existing literature is retrospective and focused

on procedural feasibility, angiographic success, or resting catheter-based gradients rather than systematic pressure-based assessment across different physiologic states.[16,17,19,20] As a result, how stent-related geometric enlargement translates into changes in Fontan hemodynamics remains poorly understood, particularly under exercise conditions when latent inefficiencies may become more pronounced.[17,18]

1.4 Need for Patient-specific Hemodynamic Evaluation

Although echocardiography, cross-sectional imaging, and catheterization remain central to Fontan surveillance, each provides only a partial view of the circulation. These modalities do not directly capture the three-dimensional relationship between pathway geometry, local flow structures, and hemodynamic inefficiency across the total cavopulmonary connection.[21] For interventions such as stenting, this limitation is especially important: the hemodynamic effect of enlarging a narrowed region depends not only on the minimum diameter achieved but on how the broader flow field is altered throughout the pathway.[21]

Computational fluid dynamics (CFD) addresses this gap by combining patient-specific anatomy from medical imaging with physics-based simulation of blood flow. Open-source platforms such as SimVascular have made this workflow increasingly accessible by integrating segmentation, geometric modeling, meshing, and hemodynamic simulation into a single pipeline.[22] Applied to the Fontan circulation, CFD has been used to quantify pressure distribution, power loss, and flow partitioning, with large cohort studies demonstrating substantial inter-patient variability even among patients with the same surgical configuration.[8]

Patient-specific simulations have also been used to support treatment planning. Surgical planning studies showed that simulation-based assessment provides useful directional insight into how geometry influences postoperative performance.[23] More recently, CFD has been applied to interventional planning for Fontan revision, including patient-specific endovascular analyses and streamlined pre-interventional workflows.[24,25] Despite this progress, the hemodynamic effect of Fontan stenting remains incompletely characterized, particularly with respect to pressure-drop changes across rest and exercise conditions in patient-specific anatomies. That

unresolved question motivates the present study.

1.5 Study objective

The hemodynamic vulnerability of the Fontan circulation, the occurrence of pathway narrowing, and the growing role of computational modeling in treatment planning together motivate a need for patient-specific evaluation of how stenting alters Fontan hemodynamics under different physiologic conditions.[8,11,12,24,25] In particular, it remains unclear whether stent-related pathway enlargement consistently reduces pressure drop, power loss, and resistance at baseline and whether any benefit is maintained or amplified during exercise, when flow demand increases and latent inefficiencies may become more apparent.[11,12,18]

To address this, we use patient-specific computational fluid dynamics simulations to investigate the hemodynamic impact of virtual stenting in three Fontan patients. For each case, pre-stent and post-stent geometries are compared under resting and exercise conditions, with primary emphasis on pressure drop, power loss, and resistance. This study is intended to evaluate feasibility, characterize within-patient trends, and provide mechanistic insight into how geometric enlargement of the Fontan pathway influences hemodynamic performance across physiologic states.[8,24,25]

2 Background

2.1 Sources of obstruction and geometric narrowing in Fontan pathways

Obstruction within the Fontan pathway may arise from discrete stenosis at or near the cavopulmonary connection, geometric distortion or kinking of the conduit, external compression, or progressive reduction in effective conduit caliber after implantation.[16,26] In extracardiac Fontan patients, this problem is compounded by the fact that the conduit does not grow with the child. Longitudinal and cross-sectional imaging studies have shown that conduit cross-sectional area can decrease

during follow-up and that many adolescents with 16–20 mm extracardiac conduits develop measurable flow acceleration from the inferior vena cava into the conduit, consistent with relative undersizing as body size and flow demand increase.[18,26,27] This effect is quantified by the IVC-to-conduit velocity mismatch factor, which is significantly greater in smaller conduits across all respiratory phases (Figure 3).

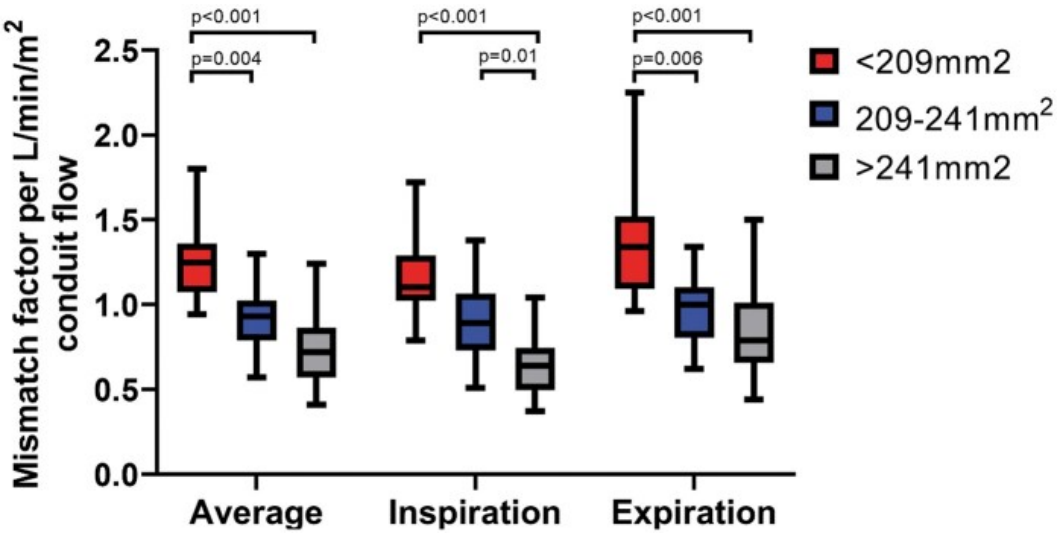

Figure 3: IVC-to-conduit velocity mismatch factor by conduit cross-sectional area group in adolescent extracardiac Fontan patients. Smaller conduits (red, <209 mm^2) show significantly greater mismatch than larger conduits (gray, >241 mm^2) across all respiratory phases, consistent with relative undersizing as body size and flow demand increase. Adapted from Rijnberg et al.[27] under CC BY-NC 4.0.

Localized narrowing is hemodynamically important because it produces a disproportionate increase in flow inefficiency. As lumen area decreases, blood velocity rises through the narrowed region, increasing viscous losses and the pressure difference required to drive flow across the pathway.[9,27] In the Fontan circulation, where pulmonary blood flow already occurs in a low-energy system, these additional losses are especially consequential. Computational studies have shown that adverse geometric features increase energy dissipation within the total cavopulmonary connection, and patient-specific upsizing analyses demonstrate that enlarging undersized conduits can reduce pressure gradients and power loss, although the magnitude of improvement remains strongly patient-specific.[9,28,29]

These findings help explain why a stenosis that appears modest on static imaging may still carry meaningful physiologic consequences. Fontan obstruction is shaped not only by minimum diameter, but also by its interaction with overall pathway geometry, inflow alignment, and flow rate. This is particularly relevant during exercise, when higher venous return may unmask losses that are less apparent at rest.[13,18,27]

2.2 Stenting in Fontan patients

Transcatheter stenting in Fontan patients is most often performed to address discrete pathway stenosis or conduit restriction identified by imaging, catheterization, or a combination of anatomic and hemodynamic findings.[16,17] Clinical reports show that the procedure is generally feasible and effectively enlarges narrowed Fontan segments, with acute reductions in measured gradients and improvement in pathway caliber after intervention.[19,20] These studies support stenting as a practical means of relieving obstruction, particularly in extracardiac conduits that become relatively undersized over time,[17,19,20] as illustrated by the representative post-procedural angiograms in Figure 4.

The current literature nonetheless leaves important questions unresolved. Most available evidence comes from retrospective series with small cohorts, and reported outcomes are often procedural or anatomic—technical success, change in conduit diameter, or immediate catheter-based gradient reduction.[19,20] These measures reflect short-term efficacy but do not characterize how stenting alters the broader hemodynamic environment of the total cavopulmonary connection, particularly pressure-drop behavior under changing physiologic demand.[17,20]

Recent computational work on Fontan conduit upsizing supports the view that pathway enlargement can improve hemodynamics, but that the magnitude and mechanism of benefit are strongly patient-specific.[29] Collectively, prior studies establish that Fontan stenting is clinically useful while underscoring the need for patient-specific assessment of how geometric enlargement translates into pressure-based and flow-based changes across different physiologic states.[17,18,20,29]

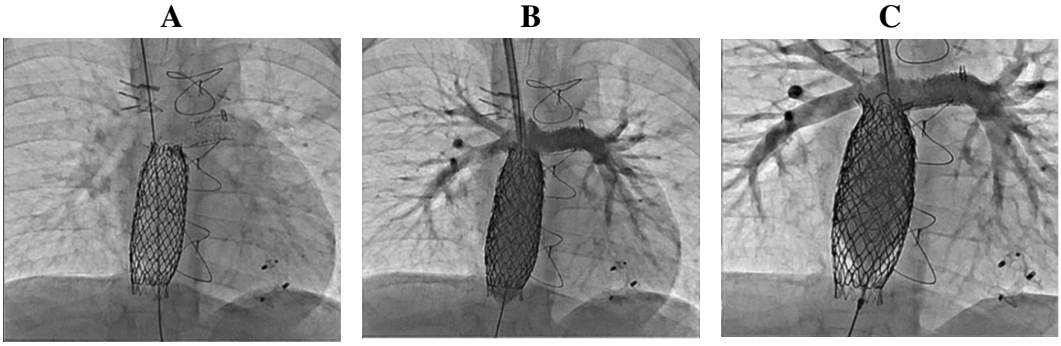

Figure 4: Representative angiographic images following Fontan pathway stenting. Panels A–C were adapted from Jalal et al.[17] Panels A–C show post-procedural angiograms after completion of the intracardiac Fontan with covered stents, demonstrating inferior vena caval drainage to the pulmonary arteries without residual restriction.

2.3 Prior computational and imaging-based studies

Patient-specific modeling has become an important tool in congenital heart disease because these lesions involve highly individualized anatomy, altered physiology, and interventions whose success often depends on geometry as much as on diagnosis.[30,31] Reviews of computational modeling in CHD have emphasized that these methods can reveal otherwise inaccessible flow features, test virtual modifications in patient-specific anatomies, and support preprocedural planning when conventional imaging is insufficient.[30] Fontan physiology has been one of the most active areas for image-based simulation because the circulation is especially sensitive to resistance, flow streaming, and pathway geometry.[30–32]

Prior Fontan CFD studies have established several recurring themes. Large cohort and patient-specific studies have quantified power loss, resistance, hepatic flow distribution, and pulmonary flow partitioning, demonstrating substantial heterogeneity even among patients with similar surgical configurations.[8,9,13] Surgical planning studies extended this work by comparing candidate Fontan geometries before intervention using patient-specific simulations, and prospective follow-up data showed that these models provide useful directional predictions, although accuracy remains sensitive to postoperative anatomy and boundary-condition assumptions.[23,32,33] Advances in 4D Flow MRI and streamlined CFD workflows

have further supported clinical translation by enabling direct comparison of in vivo flow measurements with simulation outputs and reducing computation times for pre-interventional assessment.[25,34]

Catheter-based intervention planning and post-stent Fontan assessment have been studied less extensively. Existing work shows that these applications are feasible: Tang and colleagues used patient-specific simulations to evaluate lateral tunnel Fontan stenosis with virtual stent implantation, Ahmed and colleagues performed a computational analysis of endovascular revision in a lateral tunnel Fontan, and more recent virtual surgery studies have examined extracardiac conduit expansion in adults with undersized conduits.[24,35,36] This literature nonetheless remains limited to case-specific or narrowly defined scenarios rather than systematic multi-patient comparisons focused on pressure-based outcomes across physiologic states.

2.4 Why this study matters

Prior work has established the importance of Fontan pathway energetics and demonstrated the promise of patient-specific simulation, yet important translational gaps remain between computational capability and clinically useful decision support.[8,25,30,32] The published literature on Fontan intervention planning remains limited in scope, with most studies focused on surgical planning, single-case analyses, or narrowly defined revision scenarios rather than systematic evaluation of stent-related hemodynamic change across physiologic states.[23,24,32,35,36] Small, carefully characterized studies therefore retain value for testing whether a patient-specific workflow can be applied consistently and whether it yields interpretable hemodynamic trends relevant to clinical questions.

A pilot study is well suited to this aim. By examining a small number of cases in depth, it is possible to compare pre- and post-stent geometries within each patient, isolate how pressure drop and power loss respond to geometric enlargement, and assess whether those effects differ between rest and exercise conditions.[13,18,29,35] This within-patient framework is especially useful in Fontan physiology, where anatomy and intervention response are highly heterogeneous and may not be captured by pooled averages.[8,9,36]

The present study is designed to contribute in three ways. First, it tests the feasibility of a patient-specific workflow for constructing and simulating pre- and post-stent Fontan models under multiple physiologic conditions.[22,25] Second, it provides within-patient comparisons that clarify whether stenting produces consistent reductions in pressure drop or whether benefit depends on individual anatomy and flow demand.[18,24,29,35,36] Third, it emphasizes mechanistic interpretation by linking geometric change to altered flow behavior, generating hypotheses that can inform larger studies and future use of computational modeling in Fontan intervention planning.[25,30,31]

3 Methods

3.1 Study design

This study is a patient-specific computational analysis of Fontan hemodynamics before and after virtual stenting. Fifteen Fontan patients were reconstructed in SimVascular[22] as three-dimensional anatomical models from 4D flow MRI data and reviewed using preliminary geometric and hemodynamic analysis to identify cases in which pathway enlargement was most likely to reduce pressure drop. Three patients were selected for detailed study based on this screening step.[22,25,34]

For each selected patient, paired pre-stent and post-stent anatomical models were analyzed under resting and exercise flow conditions. The post-stent models were not derived from postoperative imaging; rather, they were generated by applying a virtual stenting workflow to the patient-specific pre-stent anatomy. This design enabled controlled within-patient comparison of pressure drop, power loss, and resistance before and after geometric enlargement while holding the remaining anatomy constant.

3.2 Model generation from 4D flow MRI

4D flow MRI provided volumetric coverage of the Fontan pathway and associated vessels for each of the fifteen initial cases. Because 4D flow MRI encodes velocity

information in all three spatial directions across the cardiac cycle, it served as both an anatomical imaging source for model construction and a hemodynamic dataset for boundary-condition derivation.[22,34]

Following model reconstruction, all fifteen cases underwent preliminary geometric and hemodynamic review to identify anatomies in which pathway enlargement was most likely to reduce pressure drop. This screening step focused the study on patients with a plausible mechanistic rationale for intervention rather than on the broader Fontan population indiscriminately. Three patients were selected on the basis of this review and carried forward for paired pre-stent and post-stent simulation under resting and exercise conditions.

Patient-specific Fontan geometries were then generated using an image-based vascular modeling workflow in SimVascular.[22] The raw 4D flow MRI time series was not meshed directly; instead, a three-dimensional anatomical image volume was first selected or derived from the 4D dataset and used as the basis for segmentation and geometric reconstruction. This volume may correspond to a selected cardiac phase, a time-averaged magnitude image, or a derived angiographic dataset generated from the 4D flow data. The segmentation volume was chosen to provide the clearest delineation of the Fontan lumen and adjacent vessels, since accurate lumen definition is the critical first step in geometric reconstruction. Time-resolved velocity information from the original 4D flow MRI dataset was retained for later hemodynamic analysis, but the geometry itself was constructed from a single image volume appropriate for segmentation.

Before import into SimVascular, the selected image volume was reviewed to confirm correct orientation, voxel spacing, and field of view. The dataset was cropped to the thoracic region containing the Fontan pathway and great vessels, and additional preprocessing was performed as needed to assess lumen contrast and identify image limitations that could affect segmentation, including noise, low boundary definition, or phase-aliasing artifacts in the original 4D flow acquisition. The prepared image volume was then loaded into SimVascular as the basis for model construction.[22]

Geometric reconstruction followed the standard SimVascular workflow, which builds a three-dimensional model through path creation, cross-sectional segmenta-

tion, surface lofting, vessel unioning, and volumetric meshing. Separate centerline paths were created for each major vessel, including the superior and inferior vena cava, left and right pulmonary arteries, hepatic veins, and additional branch vessels when relevant. Each path is defined by user-placed control points from which spline-based path points are generated to represent the vessel centerline trajectory, establishing the orientation of orthogonal slice planes used for segmentation. Path placement was performed carefully to keep the centerline near the middle of the lumen, extend through the desired modeled region, and preserve overlap near junctions for robust vessel merging, as illustrated by the representative pathing shown in Figure 5.

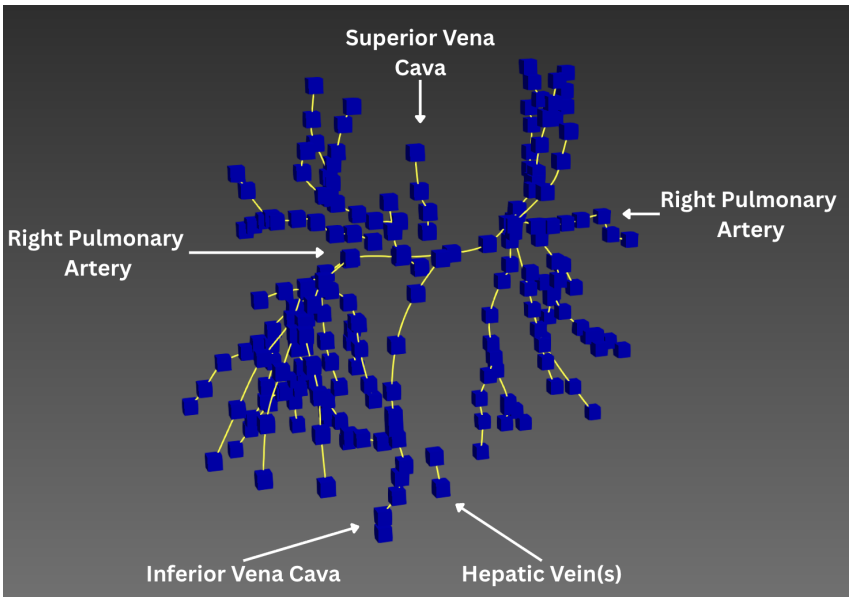

Figure 5: Representative vessel pathing for a Fontan model in SimVascular. Centerline paths were defined for the major vessels and used to orient cross-sectional planes for segmentation.

Cross-sectional lumen segmentations were then created along each path to define the vessel boundary in two-dimensional planes normal to the local centerline direction. Rather than direct thresholding of the entire image volume, the vessel is represented by a sequence of local contours sampled along the path and stitched together into a continuous three-dimensional surface. Contours were generated using

a combination of semi-automated and manual tools, including threshold-based approaches, two-dimensional level-set methods, and manual spline or polygon contours where automatic methods were inadequate. Manual correction was particularly important in regions of complex Fontan anatomy, including branch takeoffs, junctional regions, and irregular post-surgical lumen shapes, where automated contours could become inaccurate or non-physiologic; a representative segmentation sequence is shown in Figure 6.

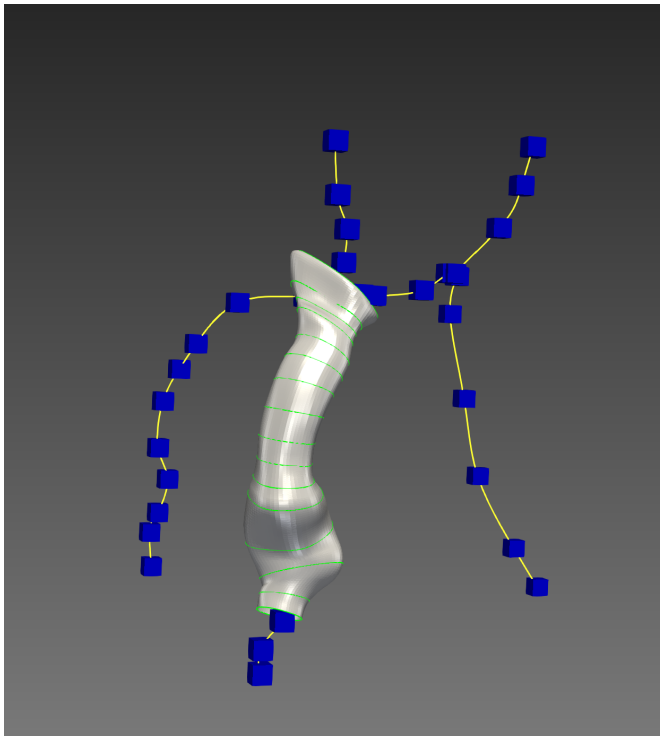

Figure 6: Representative cross-sectional segmentation along a Fontan vessel path. Local contours sampled along the centerline were used to reconstruct the three-dimensional vessel surface.

Contour spacing was chosen according to local geometric complexity. Straight vessel segments with slow changes in cross-sectional area were segmented sparsely, whereas regions with curvature, caliber change, stenosis, flare, or branch origins were segmented more densely. Each contour underwent visual inspection and editing to ensure it represented the intended lumen boundary and did not inadvertently include adjacent branch vessels or extraneous structures. This step was particularly

important near cavopulmonary junctions and pulmonary artery origins, where a poorly defined contour can introduce lofting artifacts or non-physiologic surface bulges in the final model.

Once an acceptable contour stack had been established for a given vessel, the contours were lofted to generate an individual three-dimensional vessel surface. This process was repeated for each vessel path, and the resulting surfaces were unioned into a single connected lumen, with junctional regions blended to smooth transitions between conduit, caval, and pulmonary artery segments;[22] the resulting reconstructed anatomy is represented in Figure 7.

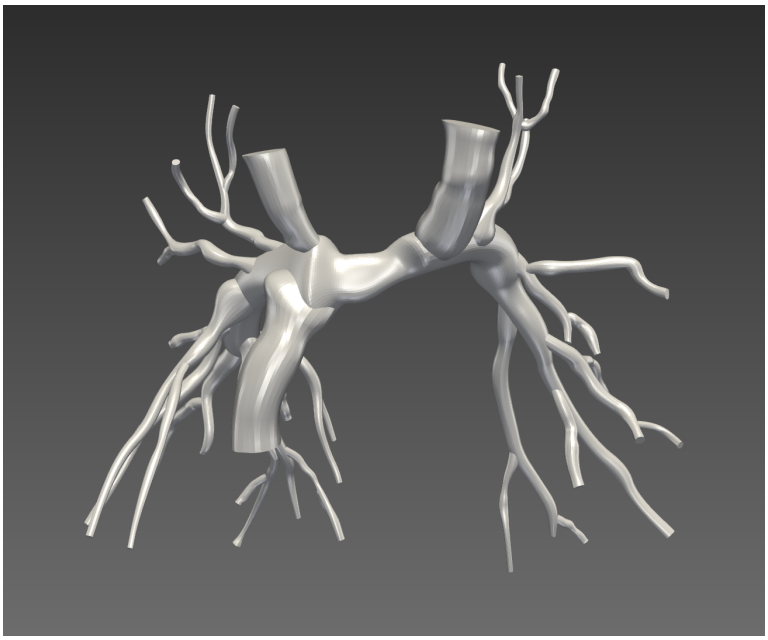

Figure 7: Representative reconstructed full Fontan model after lofting, unioning, and surface blending.

After the full surface model was assembled, vessel ends were trimmed to create clean inlets and outlets and standardize the computational domain. Truncation retained the proximal inflow and outflow vessels most relevant to Fontan hemodynamics while excluding distal anatomy outside the region of interest, reducing geometric complexity and computation time and focusing the analysis on pressure loss and flow behavior attributable to the Fontan pathway itself. The open ends were then capped, and distinct surface faces were created for the vessel wall and each inlet

and outlet to generate a watertight simulation domain, as shown for a representative case in Figure 8.

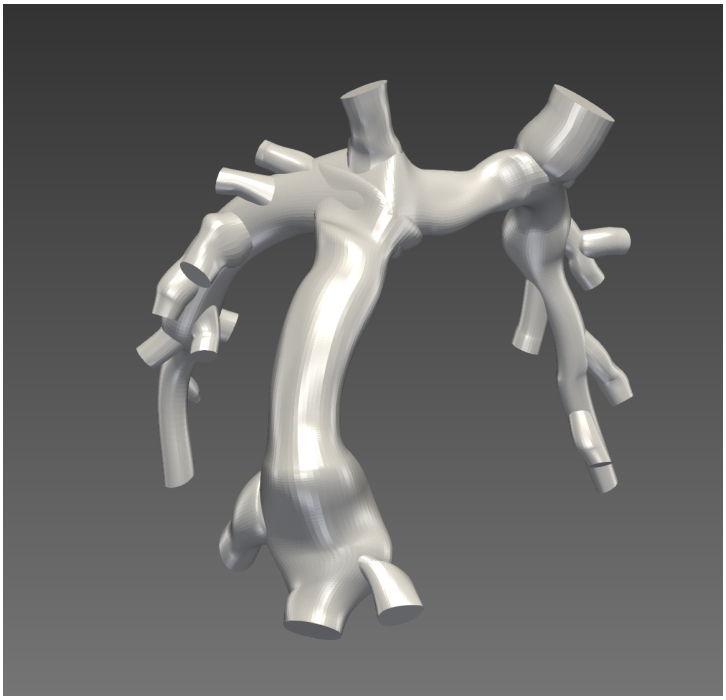

Figure 8: Representative truncated Fontan model after trimming and capping of inlet and outlet boundaries.

The completed surface model was inspected in three dimensions for geometric quality, including irregularities from poor contour definition, abrupt local kinks, non-smooth junctional transitions, unintended side pockets, incomplete caps, or other artifacts that could compromise meshing or produce non-physiologic flow features. Surface cleanup and local refinement were performed as needed until the model was suitable for volumetric meshing.

A tetrahedral volume mesh was then generated in SimVascular using TetGen.[22] Mesh density was selected to balance geometric fidelity with computational tractability, with finer resolution in regions of narrowing, curvature, and junctional complexity where velocity gradients and pressure losses were most sensitive to geometric detail. A mesh-independence study had previously been conducted within the SimVascular workflow, and the meshing conditions used here were selected

on that basis as providing an appropriate balance between numerical accuracy and computational cost. The mesh was inspected to confirm adequate resolution in narrow regions and at branch junctions, preservation of intended inlets and outlets, and absence of element quality problems. The final exported mesh included the volumetric tetrahedral domain with individual face surfaces corresponding to the vessel wall and each inlet and outlet boundary, with a representative example shown in Figure 9.

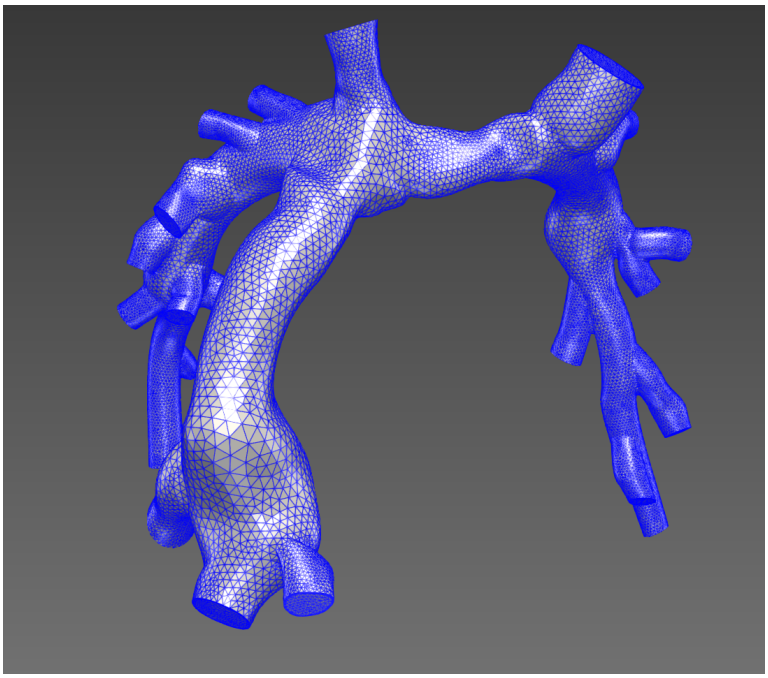

Figure 9: Representative volumetric tetrahedral mesh of a Fontan model generated in SimVascular.

3.3 Virtual stent model generation

Post-stent geometries were generated using svMorph,[37] an in-silico vascular morphing tool for interactive editing of triangulated vascular surface meshes with associated centerlines. For each selected case, a centerline of the reconstructed Fontan model was generated and exported together with the corresponding surface mesh from the SimVascular workflow. Both files were imported into the svMorph graphical interface, which uses the centerline as the geometric reference for selecting

the deformation site and defining the stent axis; a representative example of the extracted centerline is shown in Figure 10.

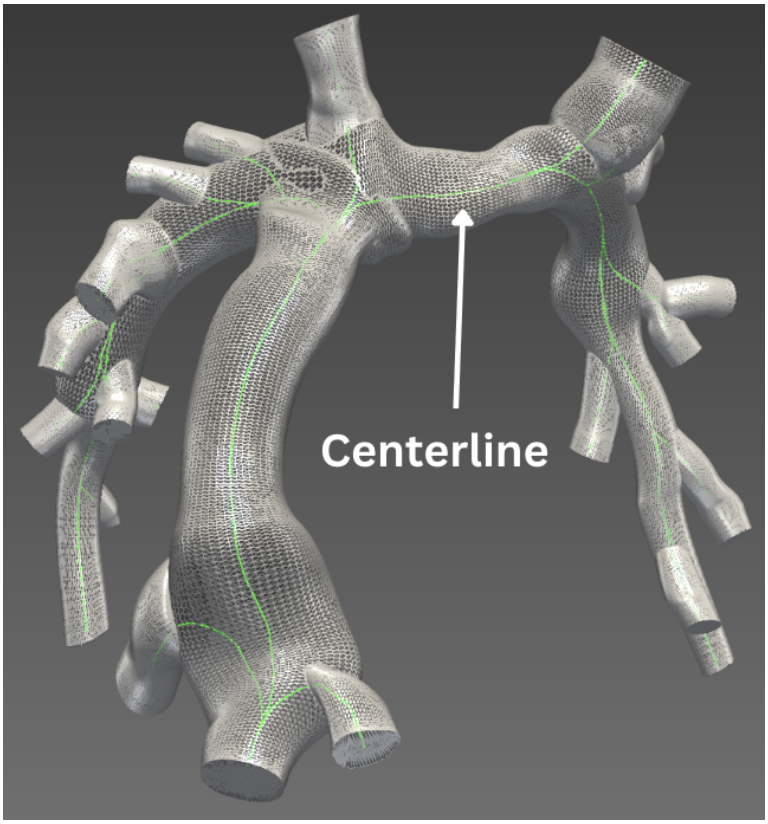

Figure 10: Representative centerline generation for a Fontan model. The extracted centerline was used as the geometric reference for subsequent virtual stent placement in svMorph.

The target site for virtual stenting was determined from the preliminary geometric and hemodynamic review used for case selection. This involved identifying the segment of the Fontan pathway most likely to contribute to elevated pressure drop, with attention to focal caliber reduction, abrupt tapering, local geometric distortion, or regions that appeared relatively undersized compared with adjacent segments. A centerline point within the target region was then selected in svMorph to initialize the virtual intervention.

Virtual stent deployment was performed using the stent-deployment mode in svMorph. Stent length and diameter were adjusted interactively, and the stent was

extended across the full length of the affected pathway to treat the entire narrowed segment. Stent diameter was increased until no obvious residual focal narrowing remained, with the goal of producing a smoother and more uniform luminal caliber along the Fontan pathway. The resulting deformed surface mesh was exported as the post-stent geometry for subsequent truncation, meshing, and computational simulation. The paired pre-stent and post-stent geometries used for hemodynamic comparison are illustrated in Figure 11.

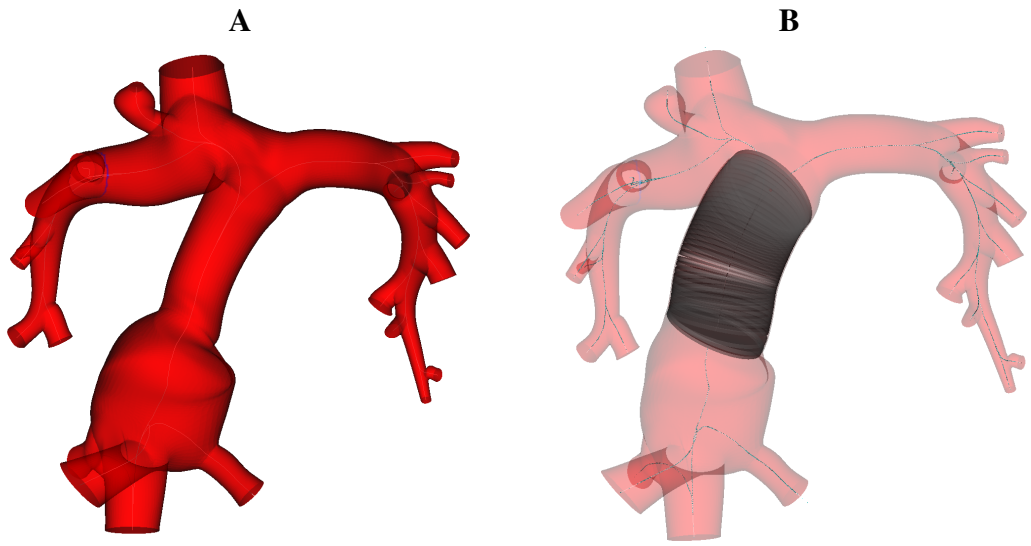

Figure 11: Representative pre-stent and post-stent Fontan models used for paired hemodynamic analysis. Panel A shows the original patient-specific geometry before virtual stent expansion. Panel B shows the corresponding post-stent geometry after virtual enlargement of the narrowed Fontan pathway.

Because the intervention was virtual, the post-stent model represents the altered luminal surface after geometric deformation rather than an explicit structural model of the deployed device. The subsequent hemodynamic analysis therefore focused on the effect of the modified pathway geometry on pressure drop, power loss, and resistance.

3.4 Simulation setup

Hemodynamic simulations were performed on the pre-stent and post-stent Fontan geometries using the SimVascular finite-element solver framework.[22]

Simulations were run as transient three-dimensional fluid solves using 32,000 time steps of size 0.001 s, resolving pulsatile pressure and velocity changes throughout the cardiac cycle. The fluid equations were solved in a fully coupled manner at each time step using a stabilized transient formulation. Each time step was iteratively converged with a minimum of 2 and maximum of 7 nonlinear iterations and a convergence tolerance of 10^{-4}, and linearized subproblems were solved using a Krylov-based sparse linear algebra framework. Backflow stabilization was included to improve numerical robustness near outlet boundaries, where local recirculation and transient reverse flow are not uncommon in complex Fontan geometries.

Blood was modeled as an incompressible Newtonian fluid with density $\rho = 1.06$ g/cm^3 and dynamic viscosity $\mu = 0.04$ P. Vessel walls were assumed rigid, with a no-slip condition applied at the wall surface. Wall compliance, vessel motion, and fluid–structure interaction were therefore not included. These assumptions are standard in large-vessel cardiovascular CFD and are appropriate for isolating the influence of pathway geometry on pressure loss and flow transport.[22]

Unsteady inflow boundary conditions were prescribed at the venous inlet faces using imposed-flux waveforms. At each inlet, the solver imposed the instantaneous volumetric flux through a parabolic velocity profile, preserving pulsatility while ensuring that integrated inflow matched the target waveform at every time step. Distal outlet boundary conditions were represented using branch-specific three-element Windkessel models of RCR type, each consisting of a proximal resistance, distal resistance, capacitance, distal pressure, and initial pressure. This multiscale formulation represented the aggregate hemodynamic effect of the distal pulmonary vasculature, which was not explicitly included in the truncated three-dimensional geometry, coupling the patient-specific Fontan domain to reduced-order downstream vascular loading.

To assess physiologic fidelity, the patient-specific simulations were validated against available clinical data by matching the simulated left-to-right pulmonary artery flow split to 4D flow MRI measurements and the average Fontan pressure to

catheterization reports. In practice, this meant that the boundary-condition setup was tuned so that the simulated LPA/RPA flow distribution agreed with the measured pulmonary flow split, while the cycle-averaged Fontan pressure level remained consistent with the reported catheterization pressure data. This validation step was used to ensure that the simulated hemodynamics were grounded in both the patient-specific anatomy and the available in vivo flow and pressure measurements.

3.5 Exercise conditions

Each selected Fontan model was simulated under both resting and exercise conditions to evaluate the effect of virtual stenting under increased physiologic demand. Exercise-state boundary conditions were prescribed using an approach informed by prior patient-specific Fontan simulations in which exercise was represented within a three-dimensional CFD framework by increasing venous inflow and reducing downstream pulmonary resistance.[38,39]

Only one exercise state was used in the present study, corresponding to a moderate exercise condition. Relative to the resting case, mean IVC inflow was multiplied by 3.0, mean SVC inflow was kept at 1.0 times its resting value, and distal pulmonary resistance values at the outlet boundary conditions were reduced by 10%. These scaling factors follow the moderate-exercise prescription used in prior Fontan CFD studies, where light, moderate, and heavy exercise were modeled by increasing IVC flow by 2×, 3×, and 4× resting flow, leaving SVC flow unchanged for light and moderate exercise, increasing SVC flow by 50% only in heavy exercise, and reducing outlet resistances by 5%, 10%, and 15%, respectively.[39]

In addition to these flow and resistance changes, the inflow waveform was temporally scaled according to heart rate. For the moderate exercise case, the cardiac rate was set to 120 beats per minute, consistent with the exercise scaling used in the reference study.[39] Thus, the exercise simulations in the present work reflect a physiologically motivated increase in venous return, reduced downstream pulmonary vascular loading, and a shortened cardiac cycle relative to rest.

This exercise-state prescription was chosen to test whether geometric enlargement through virtual stenting had a different hemodynamic effect once flow demand

increased and latent inefficiencies became more apparent.[13,14,39] The exercise simulations should therefore be interpreted as a standardized moderate physiologic stress condition rather than as a patient-specific prediction of peak exercise performance.

3.6 Definition of hemodynamic metrics

The primary hemodynamic outcomes evaluated from the transient simulations were pressure drop across the Fontan pathway, power loss within the reconstructed domain, and resistance.[8,9,13]

All reported hemodynamic quantities were computed as time-averaged values over the cardiac cycle rather than from a single instantaneous time point. Specifically, results were extracted from the sixth cardiac cycle after the start of the simulation, since the pulmonary flow split had converged before that point and the sixth cycle therefore provided a consistent basis for comparison across cases and conditions.

Pressure drop was defined using area-averaged pressure values at the truncated inlet and outlet boundaries. Pressure was extracted at the venous inflow face or faces and at the pulmonary outlet face or faces, and the pressure drop across the Fontan pathway was calculated as

$$\Delta P = \bar{P}_{\text{in}} - \bar{P}_{\text{out}},$$

where $\bar{P}_{\text{in}}$ and $\bar{P}_{\text{out}}$ denote the area-averaged pressures at the inflow and outflow boundaries, respectively. When multiple inflow or outlet faces were present, pressures were combined using a consistent branchwise averaging scheme.

Resistance was not taken directly from the CFD solver, but was calculated from the simulated pressure drop and flow rate as

$$R = \frac{\Delta P}{Q},$$

where ΔP is the pressure drop across the Fontan pathway and Q is the corresponding volumetric flow rate. Resistance was computed from the cycle-averaged pressure drop and total flow through the Fontan pathway. When expressed in cgs units, with pressure in dyn/cm^2 and flow in cm^3/s, resistance has units of $\text{dyn} \cdot \text{s}/\text{cm}^5$. This metric provides a compact summary of the effective opposition to flow imposed by

the pathway and was used alongside pressure drop and power loss to characterize the hemodynamic effect of virtual stenting.

To place the simulated pathway resistance in clinical context, effective Fontan pathway resistance was also expressed as a percentage of pulmonary vascular resistance (PVR), calculated as

$$R_{\%\mathrm{PVR}} = \frac{R}{\mathrm{PVR}} \times 100.$$

Patient-specific PVR values were obtained from catheterization data and were 1.7, 2.3, and 1.6 Wood units for Patients 18, 21, and 23, respectively. These were converted to cgs units using

$$1\ \mathrm{WU} = 80\ \mathrm{dyn} \cdot \mathrm{s/cm}^5,$$

yielding PVR values of 136, 184, and 128 $\mathrm{dyn} \cdot \mathrm{s/cm}^5$, respectively. Reporting effective resistance as a percentage of PVR provides an interpretable measure of how much of the total pulmonary vascular resistance burden is attributable to the Fontan pathway itself.

Power loss was defined as the difference between the total mechanical energy flux entering and leaving the three-dimensional model domain. In compact form, the mechanical energy flux across a boundary face can be written as

$$\int_A \left(p + \frac{1}{2}\rho|\mathbf{u}|^2 \right) (\mathbf{u} \cdot \mathbf{n})\, dA,$$

so that power loss across the Fontan model was calculated as

$$PL = \sum_{\text{inlets}} \int_A \left(p + \frac{1}{2}\rho|\mathbf{u}|^2 \right) (\mathbf{u} \cdot \mathbf{n})\, dA - \sum_{\text{outlets}} \int_A \left(p + \frac{1}{2}\rho|\mathbf{u}|^2 \right) (\mathbf{u} \cdot \mathbf{n})\, dA,$$

where p is pressure, ρ is fluid density, $\mathbf{u}$ is velocity, and $\mathbf{n}$ is the outward unit normal. This quantity reflects the mechanical energy dissipated by viscous and geometric losses as blood traverses the Fontan connection and is a useful descriptor of pathway efficiency beyond pressure difference alone.[9,13] Power loss was assessed

alongside pressure drop and resistance under both rest and exercise conditions given the particular sensitivity of Fontan hemodynamics to dissipation at higher flows.[9,13]

Together, these metrics capture complementary aspects of Fontan performance. Pressure drop, resistance, and power loss characterize the pressure burden, effective opposition to flow, and energetic cost of blood transport through the pathway. Reporting effective resistance as a percentage of PVR further places the simulated pathway burden in the context of the overall pulmonary vascular resistance load. Evaluating all three measures allowed the effect of virtual stenting to be interpreted in terms of reduced obstruction and improved pathway efficiency.[8,9,13]

4 Results

4.1 Cohort and model summary

Results are reported for three Fontan patients using paired pre-stent and post-stent models under resting and exercise conditions. For each patient, the analysis framework therefore consisted of four simulation states: rest without stent, rest with stent, exercise without stent, and exercise with stent.

The three cases differed in ways relevant to interpretation of the hemodynamic results. Patient 18 had more complex venous anatomy, including substantial azygous return and prior surgical connection of the hepatic veins to the Fontan graft. As a result, flow through the IVC pathway did not represent the entirety of venous return in the same straightforward way as in the other two cases, and changes to the stented segment could alter downstream flow organization in the presence of competing venous streams. In contrast, Patients 21 and 23 showed a more conventional pattern of focal Fontan pathway narrowing and therefore served as more straightforward cases for evaluating the hemodynamic effect of virtual pathway enlargement. The pre-stent geometries, virtual stenting setup, and resulting post-stent geometries for the three study patients are shown in Figure 12.

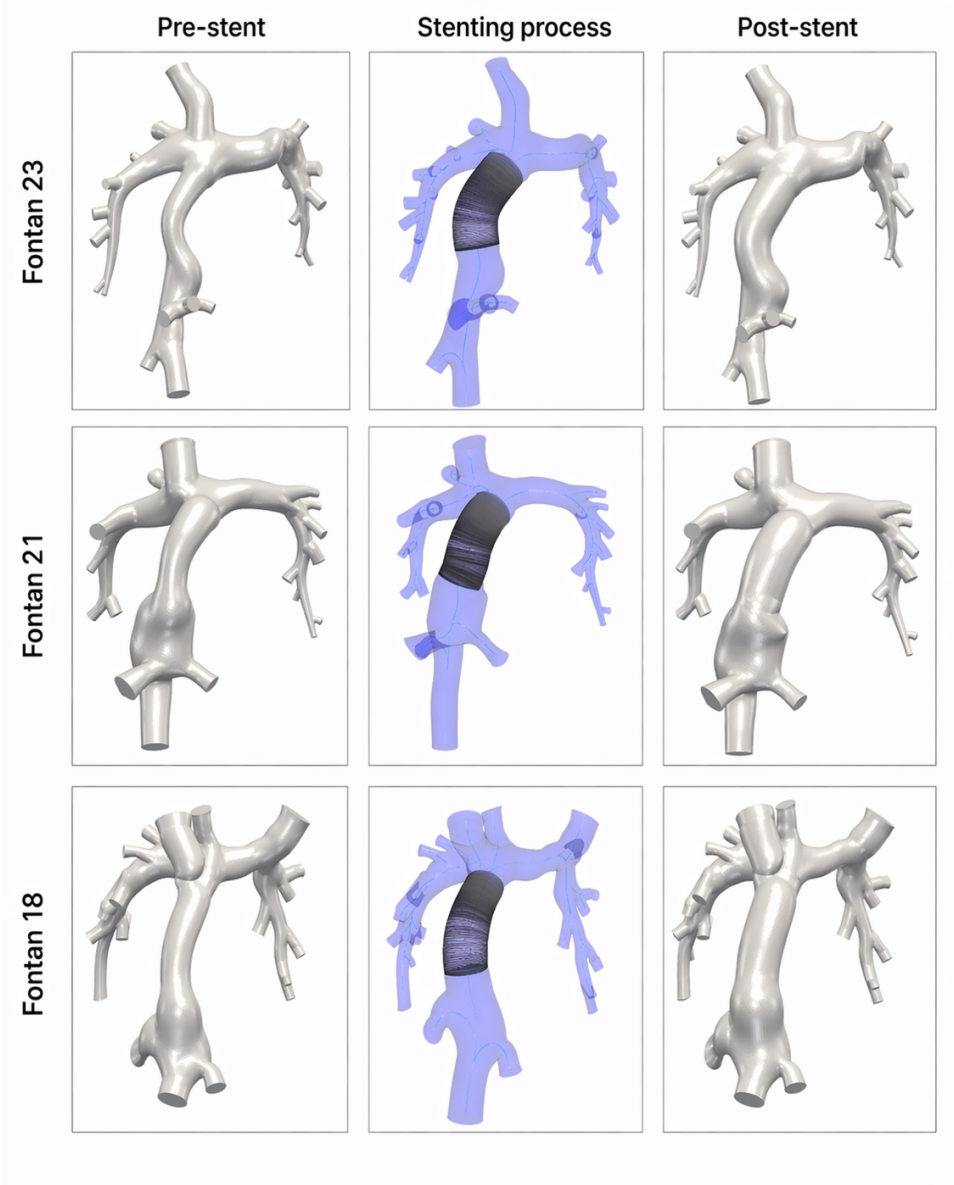

Figure 12: Comparison of pre-stent geometry, stenting process, and post-stent geometry for the three Fontan cases included in this study. Each row corresponds to one patient, and each column shows the pre-stent model, the virtual stenting setup, and the resulting post-stent model, respectively.

4.2 Feasibility of the patient-specific workflow

For all three cases, the workflow produced paired pre-stent and post-stent geometries that could be simulated under both resting and exercise conditions, enabling direct within-patient comparison across the four simulation states.

Feasibility was therefore not limited by whether the pipeline could be completed, but rather by how straightforwardly the resulting hemodynamics could be interpreted. In particular, the more complex venous anatomy in Patient 18 made interpretation less direct than in Patients 21 and 23, which had more conventional focal Fontan pathway narrowing. Overall, these results support the feasibility of the patient-specific modeling and virtual stenting pipeline while also highlighting that interpretation remains sensitive to patient-specific anatomy.

4.3 Pressure drop, power loss, and resistance before and after stenting at rest

At rest, the hemodynamic effect of virtual stenting differed across patients and is reported here using pressure drop, power loss, and resistance. Pressure drop reflects the local pressure burden across the Fontan pathway, power loss reflects the energetic cost of blood transport, and resistance provides a summary measure of the effective opposition to flow under the prescribed boundary conditions. To place pathway resistance in clinical context, effective resistance was also reported as a percentage of pulmonary vascular resistance (PVR). All reported values correspond to cycle-averaged quantities extracted from the sixth cardiac cycle. Pressure drop was computed from area-averaged pressures evaluated at the inlet and outlet measurement planes shown in Figure 13 for a representative case.

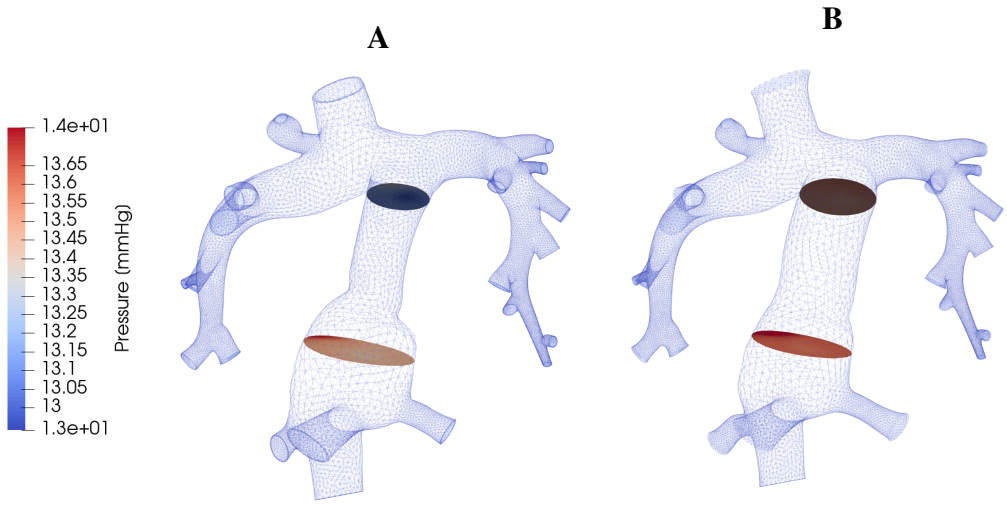

Figure 13: Measurement planes used to compute pressure drop for Patient 21. Panel A shows the pre-stent geometry and Panel B shows the post-stent geometry. Pressure drop was calculated from the area-averaged pressures at the indicated inlet and outlet planes. The color bar denotes pressure in mmHg.

For Patient 18, resting pressure drop decreased from 0.240 mmHg in the pre-stent model to 0.0682 mmHg in the post-stent model, corresponding to an absolute decrease of 0.172 mmHg and a relative reduction of 71.6%. Power loss increased from 0.000267 W to 0.000343 W, corresponding to a relative increase of 28.5%. Resistance decreased from 38.38 to 2.41, corresponding to a relative reduction of 93.7%. Expressed relative to PVR, effective pathway resistance decreased from 28.2% to 1.8% of PVR. Thus, in Patient 18, the resting response was mixed, with improvement in pressure drop and resistance but a slight increase in power loss.

For Patient 21, pressure drop decreased from 0.510 mmHg in the pre-stent model to 0.100 mmHg in the post-stent model, corresponding to an absolute decrease of 0.410 mmHg and a relative reduction of 80.5%. Power loss decreased from 0.002309 W to 0.001315 W, corresponding to a relative reduction of 43.0%. Resistance decreased from 20.03 to 1.34, corresponding to a relative reduction of 93.3%. Expressed relative to PVR, effective pathway resistance decreased from 10.9% to 0.7% of PVR.

For Patient 23, pressure drop decreased from 0.217 mmHg in the pre-stent model to 0.0284 mmHg in the post-stent model, corresponding to an absolute

decrease of 0.189 mmHg and a relative reduction of 86.9%. Power loss decreased from 0.000597 W to 0.000372 W, corresponding to a relative reduction of 37.7%. Resistance decreased from 14.03 to 0.384, corresponding to a relative reduction of 97.3%. Expressed relative to PVR, effective pathway resistance decreased from 11.0% to 0.3% of PVR.

Across the three patients, resting pressure drop and resistance decreased after virtual stenting in all cases, while the change in power loss was not uniform. Resting hemodynamic results are summarized in Table 1 and Figure 14.

Table 1: Pressure drop, power loss, resistance, and effective resistance as a percentage of pulmonary vascular resistance (PVR) at rest before and after virtual stenting. Resistance is reported in dyn · s/cm^5.

	Pressure drop [mmHg]			Power loss [W]			Resistance [dyn · s/cm^5]			Effective resistance as % of PVR	
Patient	Pre	Post	%Δ	Pre	Post	%Δ	Pre	Post	%Δ	Pre	Post
18	0.240	0.0682	-71.6%	0.000267	0.000343	+28.5%	38.38	2.41	-93.7%	28.2%	1.8%
21	0.510	0.100	-80.5%	0.002309	0.001315	-43.0%	20.03	1.34	-93.3%	10.9%	0.7%
23	0.217	0.0284	-86.9%	0.000597	0.000372	-37.7%	14.03	0.384	-97.3%	11.0%	0.3%

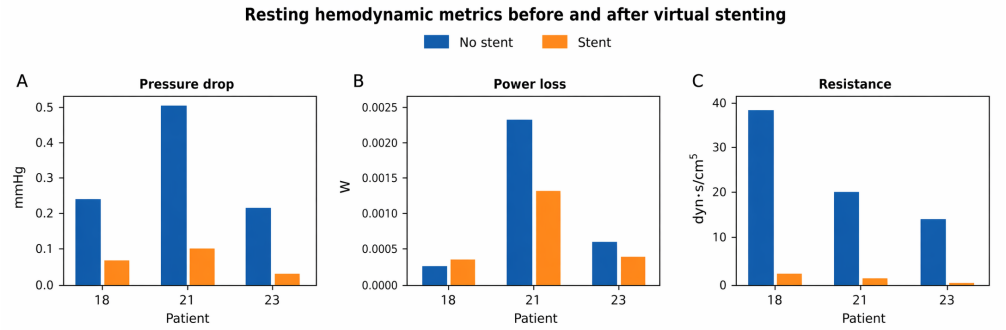

Figure 14: Summary plot of resting pressure drop, power loss, and resistance for Patients 18, 21, and 23, comparing no-stent and stent conditions.

4.4 Pressure drop, power loss, and resistance before and after stenting during exercise

Under exercise conditions, the hemodynamic effect of virtual stenting again differed across patients and is reported here using pressure drop, power loss, and resistance.

Evaluating these three metrics together provides a clearer picture of whether virtual enlargement improved Fontan pathway performance under higher-flow conditions. To place pathway resistance in clinical context, effective resistance was also reported as a percentage of pulmonary vascular resistance (PVR). As in the resting analysis, all reported values correspond to cycle-averaged quantities extracted from the sixth cardiac cycle.

For Patient 18, pressure drop decreased from 0.292 mmHg in the pre-stent model to 0.192 mmHg in the post-stent model, corresponding to an absolute decrease of 0.101 mmHg and a relative reduction of 34.4%. Power loss increased from 0.000543 W to 0.000790 W, corresponding to a relative increase of 45.6%. Resistance decreased from 28.00 to 8.28, corresponding to a relative reduction of 70.4%. Expressed relative to PVR, effective pathway resistance decreased from 20.6% to 6.1% of PVR. Thus, although virtual stenting reduced pressure drop and resistance in Patient 18, it was associated with a higher power loss under exercise.

For Patient 21, pressure drop decreased from 2.115 mmHg in the pre-stent model to 0.231 mmHg in the post-stent model, corresponding to an absolute decrease of 1.884 mmHg and a relative reduction of 89.1%. Power loss decreased from 0.0452 W to 0.0283 W, corresponding to a relative reduction of 37.3%. Resistance decreased from 17.61 to 0.334, corresponding to a relative reduction of 98.1%. Expressed relative to PVR, effective pathway resistance decreased from 9.6% to 0.2% of PVR.

For Patient 23, pressure drop decreased from 0.903 mmHg in the pre-stent model to 0.0190 mmHg in the post-stent model, corresponding to an absolute decrease of 0.884 mmHg and a relative reduction of 97.9%. Power loss decreased from 0.009337 W to 0.008508 W, corresponding to a relative reduction of 8.9%. Resistance decreased from 15.53 to 0.0758, corresponding to a relative reduction of 99.5%. Expressed relative to PVR, effective pathway resistance decreased from 12.1% to 0.06% of PVR. Representative pressure distributions for Patient 23 under exercise conditions before and after virtual stenting are shown in Figure 15.

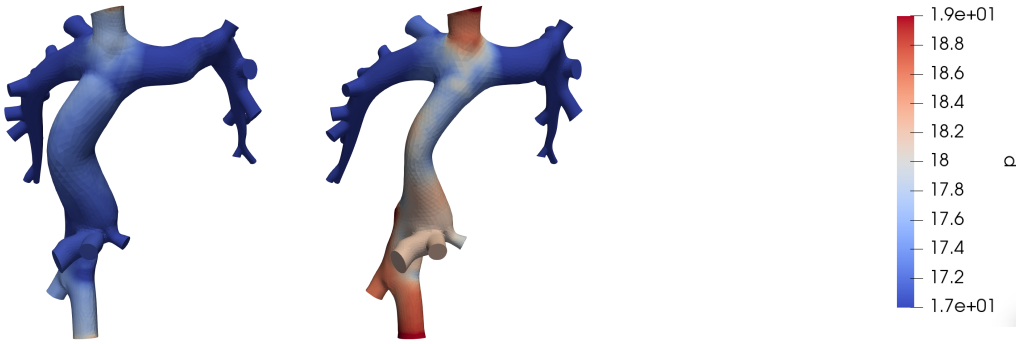

Figure 15: Pressure distribution for Patient 23 under exercise conditions before and after virtual stenting. The post-stent model (left) shows a more uniform pressure field than the pre-stent model (right), consistent with the reduction in pressure drop after virtual enlargement. The color bar denotes pressure in mmHg.

Across the three patients, exercise pressure drop and resistance decreased after virtual stenting in all cases, while the change in power loss was not uniform. Exercise hemodynamic results are summarized in Table 2 and Figure 16.

Table 2: Pressure drop, power loss, resistance, and effective resistance as a percentage of pulmonary vascular resistance (PVR) during exercise before and after virtual stenting. Resistance is reported in dyn $\cdot$ s/cm^5.

	Pressure drop [mmHg]			Power loss [W]			Resistance [dyn $\cdot$ s/cm^5]			Effective resistance as % of PVR	
Patient	Pre	Post	%Δ	Pre	Post	%Δ	Pre	Post	%Δ	Pre	Post
18	0.292	0.192	-34.4%	0.000543	0.000790	+45.6%	28.00	8.28	-70.4%	20.6%	6.1%
21	2.115	0.231	-89.1%	0.0452	0.0283	-37.3%	17.61	0.334	-98.1%	9.6%	0.2%
23	0.903	0.0190	-97.9%	0.009337	0.008508	-8.9%	15.53	0.0758	-99.5%	12.1%	0.06%

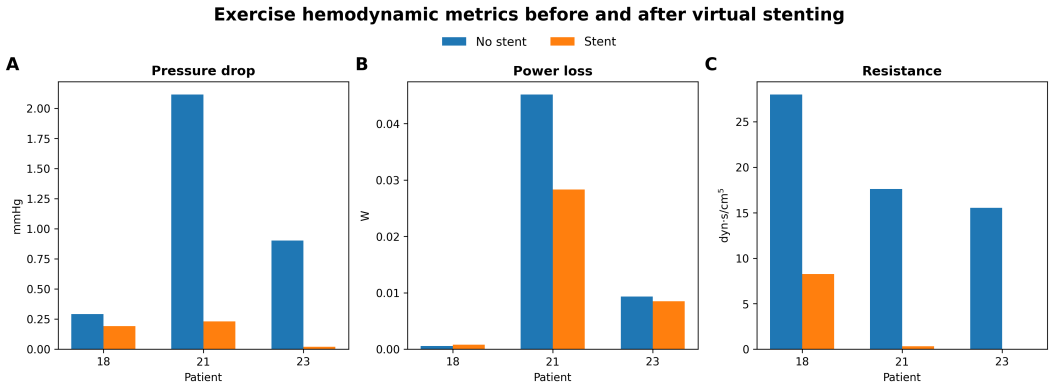

Figure 16: Exercise hemodynamic metrics before and after virtual stenting. Panel A shows pressure drop, Panel B shows power loss, and Panel C shows resistance for Patients 18, 21, and 23 under exercise conditions, comparing no-stent and stent models.

4.5 Rest-versus-exercise effect of stenting

Direct comparison of resting and exercise results showed that the hemodynamic effect of virtual stenting depended on physiologic demand and was not fully captured by a single metric. Pressure drop, power loss, and resistance together provide a more complete view of how stenting altered Fontan pathway performance across physiologic states. Effective pathway resistance was also reported as a percentage of pulmonary vascular resistance (PVR) in Tables 1 and 2 to place the simulated pathway burden in clinical context. Because this quantity is obtained by normalizing effective resistance to a patient-specific constant, its relative pre/post changes mirror those reported for resistance. All comparisons reported below are based on cycle-averaged quantities extracted from the sixth cardiac cycle of each simulation.

For Patient 18, virtual stenting reduced resting pressure drop from 0.240 mmHg to 0.068 mmHg, corresponding to a relative decrease of 71.6%. Resting power loss increased from 0.000267 W to 0.000343 W, corresponding to a relative increase of 28.5%, while resistance decreased from 38.38 to 2.41, corresponding to a relative reduction of 93.7%. During exercise, pressure drop decreased from 0.292 mmHg to 0.192 mmHg, corresponding to a relative reduction of 34.4%; power loss increased from 0.000543 W to 0.000790 W, corresponding to a relative increase of 45.6%;

and resistance decreased from 28.00 to 8.28, corresponding to a relative reduction of 70.4%.

For Patient 21, virtual stenting reduced resting pressure drop from 0.510 mmHg to 0.100 mmHg, corresponding to a relative decrease of 80.5%. Resting power loss decreased from 0.002309 W to 0.001315 W, corresponding to a relative decrease of 43.0%, and resistance decreased from 20.03 to 1.34, corresponding to a relative reduction of 93.3%. During exercise, pressure drop decreased from 2.115 mmHg to 0.231 mmHg, corresponding to a relative reduction of 89.1%; power loss decreased from 0.045176 W to 0.028333 W, corresponding to a relative reduction of 37.3%; and resistance decreased from 17.61 to 0.334, corresponding to a relative reduction of 98.1%.

For Patient 23, virtual stenting reduced resting pressure drop from 0.217 mmHg to 0.028 mmHg, corresponding to a relative decrease of 86.9%. Resting power loss decreased from 0.000597 W to 0.000372 W, corresponding to a relative decrease of 37.7%, and resistance decreased from 14.03 to 0.384, corresponding to a relative reduction of 97.3%. During exercise, pressure drop decreased from 0.903 mmHg to 0.019 mmHg, corresponding to a relative reduction of 97.9%; power loss decreased from 0.009337 W to 0.008508 W, corresponding to a relative reduction of 8.9%; and resistance decreased from 15.53 to 0.0076, corresponding to a relative reduction of 99.95%.

Overall, the rest-versus-exercise comparison showed that the magnitude of stent-related change varied by both patient and metric. In all three patients, pressure drop and resistance decreased after virtual stenting at both rest and exercise. In contrast, the magnitude and direction of change in power loss differed across patients and physiologic states. These comparisons are summarized in Table 3 and Figure 17.

Table 3: Comparison of percent change in pressure drop, power loss, and resistance after virtual stenting at rest and during exercise. Resistance is reported in $\mathrm{dyn} \cdot \mathrm{s/cm}^5$.

	Pressure drop %Δ		Power loss %Δ		Resistance %Δ	
Patient	Rest	Exercise	Rest	Exercise	Rest	Exercise
18	-71.6%	-34.4%	+28.5%	+45.6%	-93.7%	-70.4%
21	-80.5%	-89.1%	-43.0%	-37.3%	-93.3%	-98.1%
23	-86.9%	-97.9%	-37.7%	-8.9%	-97.3%	-99.95%

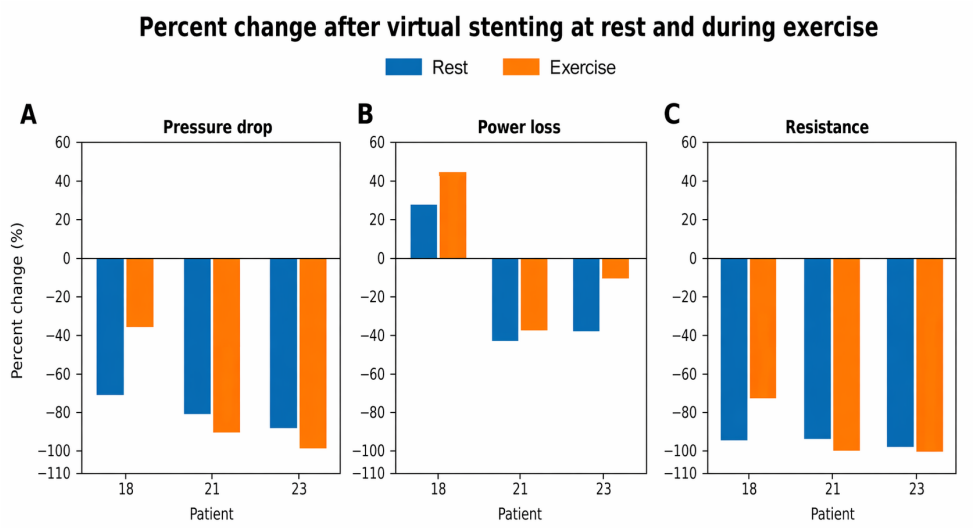

Figure 17: Comparison of stent-related percent change in pressure drop, power loss, and resistance at rest and during exercise for Patients 18, 21, and 23.

4.6 Summary of key findings

Across the three patients, virtual stenting altered Fontan hemodynamics in a patient-specific manner. At rest, pressure drop and resistance decreased after stenting in all cases. Power loss also decreased in Patients 21 and 23, but increased in Patient 18. Under exercise conditions, pressure drop and resistance again decreased in all three patients, whereas power loss decreased in Patients 21 and 23 but increased in Patient 18.

Patients 21 and 23 showed the most consistent overall improvement across metrics. In both patients, virtual stenting reduced pressure drop, power loss, and

resistance at rest and during exercise, with particularly large reductions in exercise pressure drop and resistance. Patient 18 showed a less uniform response: although pressure drop and resistance decreased after stenting at both physiologic states, power loss increased at both rest and exercise.

Overall, these results show that the hemodynamic effect of virtual stenting was heterogeneous across the study cohort and depended on both patient-specific anatomy and physiologic condition. Across the completed cases, the most consistent changes were reductions in pressure drop and resistance, while the response of power loss was more variable.

5 Discussion

5.1 Main findings

This pilot study showed that the hemodynamic effect of virtual stenting in the Fontan circulation was strongly patient-specific. In Patients 21 and 23, virtual stenting reduced pressure drop, power loss, and resistance at both rest and during exercise. These findings indicate that, in patients with functionally important Fontan pathway narrowing, virtual enlargement can meaningfully reduce the hemodynamic burden imposed by the connection.

The magnitude of benefit also depended on physiologic state. For Patients 21 and 23, the reductions in pressure drop and resistance were more pronounced during exercise than at rest, suggesting that the adverse effect of the pre-stent geometry became more consequential at higher flow rates. Power loss also decreased in both patients at both physiologic states, although the magnitude of power-loss reduction did not increase as consistently as the reduction in pressure drop and resistance.

At the same time, the results showed that stent-related benefit was not uniform across patients or across hemodynamic metrics. Patient 18 demonstrated a less consistent response: pressure drop and resistance decreased after stenting at both rest and during exercise, but power loss increased in both conditions. In the setting of substantial azygous return, this pattern suggests that enlargement of the IVC pathway altered local flow organization and mixing in a way that improved the mean

pressure gradient without producing parallel improvement in energetic efficiency. More broadly, these results indicate that the effect of stenting cannot be inferred from anatomy alone and should instead be evaluated in the context of patient-specific flow conditions and multiple complementary hemodynamic measures.

5.2 Mechanistic interpretation

The present results are consistent with the established dependence of Fontan hemodynamics on pathway geometry and flow demand.[5,8,9] In cases such as Patients 21 and 23, where the pre-stent pathway imposed a substantial pressure burden at rest and an even larger burden during exercise, virtual enlargement likely relieved a functionally important geometric restriction. Under these conditions, increasing the effective lumen size reduced the pressure drop required to drive flow through the pathway and lowered the energetic cost of transport, as reflected by the concurrent improvement in pressure drop, power loss, and resistance.

The more mixed response in Patient 18 suggests that not all apparent narrowing carries the same hemodynamic significance. Prior Fontan studies have shown that inefficiency can arise not only from focal caliber reduction, but also from the interaction of curvature, junctional geometry, and flow alignment across the total cavopulmonary connection.[8,28] In Patient 18, pressure drop and resistance both decreased after virtual stenting, but power loss increased at both rest and during exercise.

This pattern is physically plausible because power loss depends on the total mechanical energy dissipated across the pathway, not solely on the pressure difference between the selected inlet and outlet planes. Although IVC stenting reduced the static pressure drop across the evaluated segment, the integrated mechanical power loss increased slightly. Because the IVC inflow was prescribed, this increase likely reflects changes in kinetic energy flux and local flow organization rather than increased bulk resistance. In this patient with substantial azygous return, stenting may have altered the direction of the IVC jet and its interaction with the azygous contribution, producing a more complex downstream velocity field and greater mixing despite improvement in the mean pressure gradient.

Accordingly, the Patient 18 result suggests that virtual stenting altered the internal flow organization in a way that reduced the measured pressure drop across the pathway while increasing dissipative flow features within the connection. One plausible explanation is that enlargement changed the velocity profile and redirected the incoming venous stream such that local mixing and secondary motion became more pronounced. In the setting of complex azygous anatomy, reduced resistance across the evaluated IVC segment would not necessarily translate into lower global energetic loss. More broadly, this case illustrates that a reduction in measured pressure burden does not guarantee parallel improvement in all hemodynamic metrics.

The findings also support a mechanistic role for physiologic demand. Exercise is known to amplify the hemodynamic consequences of adverse Fontan geometry, and prior computational studies have similarly shown that pressure burden and energy dissipation become more consequential at higher flows.[13–15] The stronger stent-related reduction in pressure drop and resistance seen in Patients 21 and 23 during exercise is therefore consistent with the idea that a restriction that appears modest at rest may become much more consequential under stress. At the same time, the present results suggest that the response of power loss may be more nuanced and not necessarily parallel the pressure-drop response in magnitude.

Taken together, these results suggest that the benefit of stenting is mechanistically linked to whether the treated segment is a major determinant of pathway inefficiency under the relevant flow conditions. Lumen enlargement alone should not be assumed to produce uniform hemodynamic improvement; rather, the effect of stenting depends on the interaction between local caliber, overall pathway shape, venous inflow configuration, and physiologic demand.

5.3 Clinical relevance

The clinical relevance of these findings lies primarily in what they suggest about Fontan pathway stenting as a patient-specific intervention. In practice, stenting is often considered when imaging or catheterization shows a narrowed conduit or an elevated Fontan gradient, with the expectation that enlarging the pathway will reduce resistance and improve forward venous flow.[17,19,20] The present results support that

rationale in some cases, but also suggest that the magnitude and consistency of hemodynamic benefit may vary substantially across patients.

In Patients 21 and 23, virtual stenting was associated with clear reductions in pressure drop, power loss, and resistance at both rest and during exercise, with especially large reductions in exercise pressure drop and resistance. Expressed relative to pulmonary vascular resistance, effective pathway resistance also decreased to a small fraction of total PVR after virtual stenting, supporting the interpretation that the treated segment represented a meaningful but potentially remediable component of the overall pulmonary vascular load. From a clinical perspective, this pattern is consistent with cases in which the narrowed Fontan pathway is a functionally important source of hemodynamic burden and in which stent-based enlargement could plausibly provide meaningful physiologic benefit. In contrast, the more mixed response in Patient 18 suggests that apparent narrowing alone may not be sufficient to identify a strong stenting candidate. Even if the lumen is successfully enlarged, the overall hemodynamic gain may be limited or may differ across metrics when the treated segment is not the dominant source of inefficiency within the Fontan circuit.

These findings therefore reinforce an important clinical point: the question is not simply whether a Fontan pathway can be stented, but whether a given patient is likely to benefit hemodynamically from stenting. In that sense, patient-specific simulation may be especially useful in refining the indication for intervention, complementing rather than replacing clinical imaging and catheterization.[24,25,31] Rather than treating all visible narrowing as equally important, a more individualized approach may help distinguish cases in which stenting is likely to reduce hemodynamic burden from cases in which the expected improvement is smaller or less consistent.

More broadly, these results suggest that Fontan stenting should be viewed not only as an anatomic procedure to enlarge a conduit, but as a hemodynamic intervention whose value depends on the interaction between pathway geometry, flow conditions, and physiologic demand. This may be particularly important when deciding whether to intervene in patients with modest gradients at rest, since the present results suggest that the functional significance of a narrowing may become more evident under higher-flow conditions. Reporting effective pathway resistance as a percentage of PVR may further help place the simulated burden of a candidate

lesion in clinically interpretable context.

5.4 Relation to prior work

The present findings are broadly consistent with prior work showing that Fontan pathway geometry can have a substantial and highly patient-specific effect on hemodynamics.[8,9,30] Earlier computational studies established that adverse geometric features within the total cavopulmonary connection can increase pressure burden, power loss, and resistance, and that pathway enlargement or geometric optimization can improve these quantities in selected cases.[8,28,29] In that sense, the current results support the general view that local narrowing within the Fontan pathway can impose a meaningful hemodynamic penalty and that relieving that restriction may improve pathway performance.

The current study also aligns with prior reports that the effect of Fontan intervention is not uniform across patients. Previous computational and interventional planning studies have emphasized that the same general procedure can have different hemodynamic consequences depending on anatomy, flow conditions, and the location of the treated segment.[24,32,35] The contrast between Patient 18 and Patients 21 and 23 in the present cohort is consistent with that principle: two cases showed favorable reductions across pressure drop, power loss, and resistance, whereas the third showed a more mixed response despite apparent pathway enlargement.

At the same time, this study extends prior work by directly comparing virtual stenting under both resting and exercise conditions within the same patients. Much of the existing literature on Fontan stenting focuses on procedural feasibility, conduit caliber, or resting catheter-based gradients,[19,20] whereas fewer studies have examined how the hemodynamic effect of stenting changes as physiologic demand increases. The present results suggest that this distinction matters. In Patients 21 and 23, the reduction in pressure drop and resistance was more pronounced during exercise than at rest, supporting the idea that higher-flow conditions may reveal clinically important pathway restriction more clearly than resting analysis alone.[13,14]

The present findings also complicate any assumption that increased lumen size necessarily yields uniform hemodynamic benefit. In Patient 18, stenting reduced

pressure drop and resistance at both rest and exercise but increased power loss in both conditions, indicating that geometric enlargement alone may not be sufficient to improve all aspects of pathway performance. This result underscores the importance of evaluating multiple hemodynamic metrics and suggests that the relation between anatomy and functional improvement may be more nuanced than implied by minimum diameter alone.

Overall, this study confirms the patient-specific nature of Fontan hemodynamics, supports the use of virtual intervention analysis as an extension of prior congenital CFD work, and adds evidence that the hemodynamic significance of Fontan pathway stenting may depend strongly on physiologic state as well as anatomy.

5.5 Limitations

This study has several important limitations. First, it is a pilot analysis of only three patients, and the small sample size precludes broad statistical inference. The purpose of the study was not to establish population-level estimates of stent efficacy, but rather to evaluate the feasibility of a patient-specific virtual stenting workflow and to examine whether the hemodynamic effect of pathway enlargement could differ meaningfully across cases. As a result, the present findings should be interpreted as hypothesis-generating rather than definitive.

Second, the analysis depends on several modeling assumptions that may influence the quantitative results. The simulations were performed using rigid walls, Newtonian blood properties, and prescribed inflow and outlet boundary conditions within an open-loop framework. These assumptions are common in cardiovascular CFD and useful for isolating the influence of local pathway geometry, but they do not capture the full physiologic coupling of the Fontan circulation to the rest of the body.[21,22] In particular, the open-loop model does not account for whole-body feedback between the circulation, systemic venous return, and ventricular response.

A further limitation is that the model is more reliable for predicting changes in pressure drop than for predicting changes in absolute pressure magnitude after stenting. Because the simulations were performed in an open-loop framework with prescribed boundary conditions, alleviating local pathway resistance could change

the modeled pressure level without allowing the rest of the circulation to adjust. In a more fully coupled model, changes in venous return, ventricular filling, and distal vascular loading could alter this response. As a result, the pressure-drop results are likely more robust than the absolute pressure magnitudes predicted after virtual stenting.

Third, uncertainty in anatomy reconstruction and virtual intervention generation may affect the resulting hemodynamics. Patient-specific models were derived from segmented 4D flow MRI data, and although care was taken during path creation, segmentation, lofting, truncation, and meshing, each of these steps introduces potential sources of geometric uncertainty. Similarly, the post-stent models represent idealized virtual enlargements of the pathway rather than the exact anatomy of an implanted clinical device. The simulations therefore reflect the hemodynamic consequences of the modified lumen geometry, not the full structural or procedural reality of an actual stent deployment.

Fourth, uncertainty also remains in the exercise boundary conditions. The exercise simulations were designed to represent a physiologically motivated increase in flow demand, but the exact exercise response of an individual Fontan patient may differ from the generalized assumptions used in the model. This issue is especially relevant in anatomically atypical cases such as Patient 18. As a result, although the exercise simulations are useful for comparative analysis, they should not be interpreted as exact predictions of in vivo exercise physiology.[38,39]

Finally, the present study focused primarily on pressure drop, power loss, and resistance. Other potentially relevant outcomes, including wall shear stress patterns, local recirculation, and more direct comparison to clinical symptom burden, were outside the scope of the current analysis. Taken together, these limitations suggest that the present findings should be interpreted as an initial patient-specific assessment of virtual Fontan stenting rather than as a complete account of post-intervention hemodynamics.

5.6 Future directions

Several next steps could strengthen and extend the present study. The most important is expansion to a larger cohort. A broader patient set would make it possible to assess whether the patterns observed here, including the greater apparent benefit in some geometries than others and the stronger reduction in pressure burden under exercise conditions, are reproducible across a wider range of Fontan anatomies and flow configurations.

A second priority is stronger validation against clinical data. In particular, future work should compare simulated pressure-drop changes more directly with catheter-based measurements before and after intervention. Such comparison would help determine how well the virtual stenting framework captures the hemodynamic effect of pathway enlargement in vivo and would provide a firmer basis for clinical translation.[25,33]

Additional refinement of the physiologic model is also warranted. More realistic boundary conditions, including patient-specific exercise inputs and eventually a more fully coupled representation of the circulation, could improve interpretation of the pressure response after stenting. This would be especially valuable for distinguishing changes in local pathway pressure drop from changes in absolute pressure magnitude that may depend on broader hemodynamic adaptation.

Future studies could also expand the range of evaluated outcome metrics. Although pressure drop, power loss, and resistance were the primary focus here, other measures such as wall shear stress and recirculation patterns may provide additional insight into how virtual stenting alters Fontan pathway performance. These additional metrics may be particularly useful in cases such as Patient 18, where pressure-based and energy-based measures did not improve in parallel.

Ultimately, the long-term goal is prospective use of patient-specific virtual intervention analysis in treatment planning. In that setting, a modeling workflow such as the one presented here could be used not only to simulate whether a pathway can be enlarged, but to evaluate whether a specific patient is likely to derive meaningful hemodynamic benefit from stenting before the procedure is performed.[24,25,30]

5.7 Conclusion

In this pilot study, patient-specific virtual stenting produced heterogeneous hemodynamic effects across Fontan patients. In Patients 21 and 23, virtual pathway enlargement reduced pressure drop, power loss, and resistance at both rest and during exercise, with the largest reductions in pressure drop and resistance observed during exercise. In Patient 18, the response was more mixed: pressure drop and resistance decreased, but power loss increased at both physiologic states. Taken together, these findings suggest that the benefit of Fontan pathway stenting is strongly patient-specific and may be evaluated most effectively using patient-specific computational analysis across multiple physiologic conditions.

References

[1] Y. Liu, S. Chen, L. Zühlke, G. C. Black, M. K. Choy, N. Li, and B. D. Keavney. Global birth prevalence of congenital heart defects 1970–2017: updated systematic review and meta-analysis of 260 studies. *International Journal of Epidemiology*, 48(2):455–463, 2019.

[2] P. S. Rao. Single ventricle—a comprehensive review. *Children*, 8(6):441, 2021.

[3] J. Rychik, A. M. Atz, D. S. Celermajer, et al. Evaluation and management of the child and adult with fontan circulation: A scientific statement from the american heart association. *Circulation*, 140(6):e234–e284, 2019.

[4] M. Gewillig and S. C. Brown. The fontan circulation after 45 years: update in physiology. *Heart*, 102(14):1081–1086, 2016.

[5] M. R. de Leval, P. Kilner, M. Gewillig, and C. Bull. Total cavopulmonary connection: a logical alternative to atriopulmonary connection for complex fontan operations. *Journal of Thoracic and Cardiovascular Surgery*, 96(5):682–695, 1988.

[6] G. A. Mazza, E. Gribaudo, and G. Agnoletti. The pathophysiology and complications of fontan circulation. *Acta Biomedica*, 92(5):e2021260, 2021.

[7] J. Rychik. The relentless effects of the fontan paradox. *Seminars in Thoracic and Cardiovascular Surgery: Pediatric Cardiac Surgery Annual*, 19(1):37–43, 2016.

[8] C. M. Haggerty, M. Restrepo, E. Tang, D. A. de Zélicourt, K. S. Sundareswaran, L. Mirabella, J. Bethel, K. K. Whitehead, M. A. Fogel, and A. P. Yoganathan. Fontan hemodynamics from 100 patient-specific cardiac magnetic resonance studies: A computational fluid dynamics analysis. *Journal of Thoracic and Cardiovascular Surgery*, 148(4):1481–1489, 2014.

[9] F. M. Rijnberg, M. G. Hazekamp, J. J. Wentzel, P. J. H. de Koning, J. J. M. Westenberg, M. R. M. Jongbloed, et al. Energetics of blood flow in cardiovascular disease: Concept and clinical implications of adverse energetics in patients with a fontan circulation. *Circulation*, 137(22):2393–2407, 2018.

[10] Marc Gewillig, Stephen C. Brown, Alexander van de Bruaene, and Jack Rychik. Providing a framework of principles for conceptualising the Fontan circulation. *Acta Paediatrica*, 109(4):651–658, 2020. Open access under CC BY-NC 4.0.

[11] A. K. Mahendran, J. M. Colman, J. A. Kirsh, et al. Exercise pathophysiology and testing in individuals with a fontan circulation. *CJC Pediatric and Congenital Heart Disease*, 2(3):112–123, 2023.

[12] D. J. Goldberg, C. M. Avitabile, M. G. McBride, and S. M. Paridon. Exercise capacity in the fontan circulation. *Cardiology in the Young*, 23(6):824–830, 2013.

[13] K. K. Whitehead, K. Pekkan, H. D. Kitajima, S. M. Paridon, A. P. Yoganathan, and M. A. Fogel. Nonlinear power loss during exercise in single-ventricle patients after the fontan: Insights from computational fluid dynamics. *Circulation*, 116(11 Suppl):I165–I171, 2007.

[14] S. S. M. Bossers, M. Cibis, F. J. Gijsen, et al. Computational fluid dynamics in fontan patients to evaluate power loss during simulated exercise. *Heart*, 100(9):696–701, 2014.

[15] R. H. Khiabani, K. K. Whitehead, D. Han, et al. Exercise capacity in single-ventricle patients after fontan correlates with haemodynamic energy loss in tcpc. *Heart*, 101(2):139–143, 2015.

[16] D. J. Hagler, W. R. Miranda, B. J. Haggerty, J. H. Anderson, J. N. Johnson, F. Cetta, S. M. Said, and N. W. Taggart. Fate of the fontan connection: Mechanisms of stenosis and management. *Congenital Heart Disease*, 14(4):571–581, 2019.

[17] Z. Jalal, M. Gewillig, Y. Boudjemline, P. Guérin, M. Pilati, G. Butera, S. Malekzadeh-Milani, M. Avesani, and J. B. Thambo. Transcatheter interventions in patients with a fontan circulation: Current practice and future developments. *Frontiers in Pediatrics*, 10:965989, 2022.

[18] F. M. Rijnberg, L. C. van't Hul, M. G. Hazekamp, P. J. van den Boogaard, J. F. Juffermans, H. J. Lamb, C. T. E. de Los Monteros, L. J. M. Kroft, S. Kenjereš, S. le Cessie, M. R. M. Jongbloed, J. J. M. Westenberg, and A. A. W. Roest. Haemodynamic performance of 16–20-mm extracardiac goretex conduits in adolescent fontan patients at rest and during simulated exercise. *European Journal of Cardio-Thoracic Surgery*, 63(1):ezac522, 2023.

[19] F. E. A. Udink ten Cate, U. Trieschmann, I. Germund, T. Hannes, M. Emmel, G. Bennink, and N. Sreeram. Stenting the fontan pathway in paediatric patients with obstructed extracardiac conduits. *Heart*, 103(14):1111–1116, 2017.

[20] P. Agasthi, C. C. Jain, A. C. Egbe, D. J. Hagler, A. K. Cabalka, N. W. Taggart, J. H. Anderson, F. Cetta, H. M. Connolly, L. J. Burchill, P. S. Kamath, and W. R. Miranda. Clinical outcomes of percutaneous fontan stenting in adults. *Canadian Journal of Cardiology*, 39(10):1358–1365, 2023.

[21] D. A. de Zélicourt, A. L. Marsden, M. A. Fogel, and A. P. Yoganathan. Imaging and patient-specific simulations for the fontan surgery: current methodologies and clinical applications. *Progress in Pediatric Cardiology*, 30(1-2):31–44, 2010.

[22] A. Updegrove, N. M. Wilson, J. Merkow, H. Lan, A. L. Marsden, and S. C. Shadden. Simvascular: An open source pipeline for cardiovascular simulation. *Annals of Biomedical Engineering*, 45(3):525–541, 2017.

[23] C. M. Haggerty, D. A. de Zélicourt, M. Restrepo, et al. Comparing pre- and post-operative fontan hemodynamic simulations: implications for the reliability of surgical planning. *Annals of Biomedical Engineering*, 40(12):2639–2651, 2012.

[24] Y. Ahmed, C. Tossas-Betancourt, P. A. J. van Bakel, J. M. Primeaux, W. J. Weadock, J. C. Lu, J. D. Zampi, A. Salavitabar, and C. A. Figueroa. Interventional planning for endovascular revision of a lateral tunnel fontan: A patient-specific computational analysis. *Frontiers in Physiology*, 12:718254, 2021.

[25] P. Frieberg, N. Aristokleous, P. Sjöberg, J. Töger, P. Liuba, and M. Carlsson. Computational fluid dynamics support for fontan planning in minutes, not hours: The next step in clinical pre-interventional simulations. *Journal of Cardiovascular Translational Research*, 15(4):708–720, 2022.

[26] N. D. Patel, D. Gupta, W. A. Mays, J. J. Savla, S. K. Knecht, M. E. Turner, J. T. Tretter, I. E. Vignon-Clementel, A. M. Hlavacek, and M. J. Campbell. Progression in fontan conduit stenosis and hemodynamic impact during childhood and adolescence. *Journal of Thoracic and Cardiovascular Surgery*, 162(2):374–381.e3, 2021.

[27] F. M. Rijnberg, M. G. Hazekamp, J. J. M. Westenberg, M. R. M. Jongbloed, W. A. Helbing, and A. A. W. Roest. Extracardiac conduit adequacy along the respiratory cycle in fontan patients: influence of conduit size and hemodynamics. *European Journal of Cardio-Thoracic Surgery*, 62(1):ezab478, 2022.

[28] T. Y. Hsia, F. Migliavacca, S. Pittaccio, A. Radaelli, G. Dubini, and M. R. de Leval. Computational fluid dynamic study of flow optimization in realistic models of the total cavopulmonary connections. *Journal of Surgical Research*, 116(2):305–313, 2004.

[29] V. Govindarajan, A. Sahni, E. Eickhoff, P. E. Hammer, D. M. Hoganson, R. H. Rathod, and P. J. del Nido. Biomechanics and clinical implications of fontan upsizing. *Computers in Biology and Medicine*, 183:109317, 2024.

[30] G. Biglino, C. Capelli, J. Bruse, G. M. Bosi, A. M. Taylor, and S. Schievano. Computational modelling for congenital heart disease: how far are we from clinical translation? *Heart*, 103(2):98–103, 2017.

[31] C. Capelli, E. Sauvage, G. Giusti, G. M. Bosi, H. Ntsinjana, M. Carminati, A. M. Taylor, and S. Schievano. Patient-specific simulations for planning treatment in congenital heart disease. *Interface Focus*, 8(1):20170021, 2018.

[32] P. M. Trusty, T. C. Slesnick, Z. A. Wei, J. Rossignac, K. R. Kanter, M. A. Fogel, and A. P. Yoganathan. Fontan surgical planning: previous accomplishments, current challenges, and future directions. *Journal of Cardiovascular Translational Research*, 11(2):133–144, 2018.

[33] P. M. Trusty, Z. A. Wei, T. C. Slesnick, K. R. Kanter, T. L. Spray, M. A. Fogel, and A. P. Yoganathan. The first cohort of prospective fontan surgical planning patients with follow-up data: how accurate is surgical planning? *Journal of Thoracic and Cardiovascular Surgery*, 157(3):1146–1155, 2019.

[34] G.-H. Lee, H. J. Koo, K. J. Park, D. H. Yang, and H. Ha. Characterization of baseline hemodynamics after the fontan procedure: a retrospective cohort study on the comparison of 4d flow mri and computational fluid dynamics. *Frontiers in Physiology*, 14:1199771, 2023.

[35] E. Tang, D. B. McElhinney, M. Restrepo, A. M. Valente, and A. P. Yoganathan. Haemodynamic impact of stent implantation for lateral tunnel fontan stenosis: a patient-specific computational assessment. *Cardiology in the Young*, 26:116–126, 2016.

[36] T. Y. Hut, A. A. W. Roest, D. H. K. Gaillard, M. G. Hazekamp, P. J. van den Boogaard, H. J. Lamb, et al. Virtual surgery to predict optimized conduit size for adult fontan patients with 16-mm conduits. *Interdisciplinary Cardiovascular and Thoracic Surgery*, 2023.

[37] Jeff Bohan Li. svmorph: Real-time interactive virtual stenting and vascular morphing with sdf-contact sculpting and regularized kelvinlets. Software, version 0.1.0, 2026. MIT-licensed research tool; companion paper forthcoming.

[38] Alison L. Marsden, V. Mohan Reddy, Shawn C. Shadden, Frandics P. Chan, Charles A. Taylor, and Jeffrey A. Feinstein. A new multiparameter approach

to computational simulation for fontan assessment and redesign. *Congenital Heart Disease*, 5(2):104–117, 2010.

[39] Alison L. Marsden, Irene E. Vignon-Clementel, Frandics P. Chan, Jeffrey A. Feinstein, and Charles A. Taylor. Effects of exercise and respiration on hemodynamic efficiency in cfd simulations of the total cavopulmonary connection. *Annals of Biomedical Engineering*, 35(2):250–263, 2007.